




## Article

# Design and Experimental Assessment of a Vibration Control System Driven by Low Inertia Hydrostatic Magnetorheological Actuators for Heavy Equipment

Gabrielle Mallette <sup>\*</sup>, Charles-Étienne Gauthier, Masoud Hemmatian , Jeff Denis   
and Jean-Sébastien Plante <sup>\*</sup>

CREATEK, 3IT(P2), Département de Génie Mécanique, Université de Sherbrooke, 3000 Boulevard de l'Université, Sherbrooke, QC J1K 0A5, Canada; charles-etienne.gauthier@usherbrooke.ca (C.-É.G.); jeff.denis@usherbrooke.ca (J.D.)

<sup>\*</sup> Correspondence: gabrielle.mallette@usherbrooke.ca (G.M.); jean-sebastien.plante@usherbrooke.ca (J.-S.P.)

**Abstract:** Active suspension systems for automotive vehicles were developed in the past using hydrostatic, electric, magnetic and magnetorheological (MR) technologies to control road vibrations and vehicle dynamics and thus improve ride comfort and vehicle performance. However, no such systems were developed for heavy equipment, trucks and off-highway vehicles. For instance, agricultural tractors are still equipped with minimal suspension systems causing discomfort and health problems to drivers. The high suspension loads due to the massive weight of these vehicles are a challenge since high forces are needed to achieve efficient active suspension control. This paper presents an experimentally validated feasibility study of a hydrostatic, MR clutch-driven system of actuators. The scope of this paper is to evaluate the preliminary performance of the actuator for future vibration control. The hydraulic system allows the actuators to be remotely located from the wheels or cabin of the heavy vehicle and conveniently placed on the vehicle's suspended frame. The design includes two MR clutches driven in an antagonistic configuration to push and pull on the end effector. Experiments on a laboratory prototype show that the low-inertia characteristics of the clutches allow a high blocked-output force bandwidth of 20 Hz with peak output forces exceeding 15 kN.

**Keywords:** active suspension; magnetorheological clutches; vibration control; hydrostatic system; heavy vehicles



**Citation:** Mallette, G.; Gauthier, C.-É.; Hemmatian, M.; Denis, J.; Plante, J.-S. Design and Experimental Assessment of a Vibration Control System Driven by Low Inertia Hydrostatic Magnetorheological Actuators for Heavy Equipment. *Actuators* **2023**, *12*, 407. <https://doi.org/10.3390/act12110407>

Academic Editor: Ioan Ursu

Received: 22 September 2023

Revised: 24 October 2023

Accepted: 27 October 2023

Published: 29 October 2023



**Copyright:** © 2023 by the authors. Licensee MDPI, Basel, Switzerland. This article is an open access article distributed under the terms and conditions of the Creative Commons Attribution (CC BY) license (<https://creativecommons.org/licenses/by/4.0/>).

## 1. Introduction

Heavy modern vehicles are equipped with minimal suspension systems that expose operators to whole-body vibration (WBV). A study on dump truck operators in an Indian Iron ore mine showed that every day the majority of the operators in the study (59%) were exposed to vibrations exceeding the lower limit ( $0.45 \text{ m}\cdot\text{s}^{-2}$ ) stated by ISO-2631. The effect of high WBV includes risk of back pain, knee pain, leg pain and musculoskeletal disorders [1]. Another study measured vibration transmitted to a tractor seat on different speeds and road types and showed that ISO limits are exceeded in multiple common farming conditions. Repeated exposure to WBV can result in physical damage and decrease in work performance [2]. As well as being a health hazard to operators, vibrations also strongly affect machinery reliability and part lifespan. A known example of machinery reliability is wearing of railway caused by the interaction of railway wagon wheels and rail. The lack of vibration isolation systems causes rapid rail degradation [3].

Many suspension systems were developed to dampen vibrations. Efforts were made to find a solution especially directed at the seat. Exonetik, in collaboration with Magna International, developed an active seat suspension using magnetorheological (MR) actuators capable of outputting high force with a bandwidth of 15 Hz, reducing the vibration rate within the safety limits [4]. Davies et al. studied three types of passive air-ride seats as well

as one electromagnetic active vibration-canceling (EAVC) seat on a heavy-duty semi-truck. Although the EAVC suspension offered a significant vibration reduction and the passive air-ride provided a limited reduction, these suspensions only offer a partial solution as they act as individual protective equipment and do not act directly at the vibration source to protect mechanical parts from accelerated wear [5].

Some studies assessed the performance of a frame hydraulic active suspension. Jeong-woo et al. designed an electro-hydraulic system capable of reducing 66% of roll at  $4.9 \text{ m}\cdot\text{s}^{-2}$  lateral acceleration. The system consists of a hydraulic pump and dual racks and pinions powered by a brushless electric motor capable of controlling active height at a frequency of approximately 1 to 2 Hz [6]. However, this bandwidth is not sufficient to achieve efficient vibration control of the vehicle. Frequencies in the range of 1 to 20 Hz can cause damage to the human body [7]. The motorsport industry also tried to introduce active hydraulic suspensions. Mercedes-Benz introduced an active electronically hydro-pneumatic suspension using high hydraulic pressure and an accumulator. In this, an electronic unit computes sensor data from the vehicle dynamics and operates hydraulic servos located at each wheel of the vehicle, damping vehicle frequencies up to 5 Hz [8]. Even though active hydraulic suspension can provide high force, the maximal bandwidth is not sufficient for vibration control of damaging frequencies to the human body.

MR clutch actuators are a recent technology proven to have significant potential for vibration reduction applications. MR actuators were first introduced as magnetorheological “brakes” (not clutches) coupled with direct current (DC) motors using a three-port differential system to enhance safety and performance in robotics [9]. MR actuators evolved into “clutch” systems, where clutches are mounted in combination with electric motors and reduction gearing for use in robotics, automotive and aerospace applications. The use of MR clutches coupled with hydrostatic actuation can relocate actuators and generate high forces at high bandwidths such as those demonstrated in wearable haptic robots [10]. An MR clutch is composed of an input rotor, an output rotor, as well as a coil as illustrated in Figure 1. This drum-type clutch is developed by Exonetik Inc. (Sherbrooke, QC, Canada). (US 2018/0156285) and is capable of outputting 37 N·m, making it a viable option for high-power applications. The clutch input and output rotors are made of thin steel drums that fit one in the other, leaving a void between the drums. The void between the input and output drums is filled with magnetorheological fluid (MRF). MRF is composed of oil and iron particles, making it a fluid that has the characteristic to change viscosity as a function of the magnetic field passing through it. The coil mounted in the clutch assembly allows the magnitude of the magnetic field to be modified easily. Therefore, MR clutches work by transmitting torque through the shear surface of the MR fluid. The transferred torque varies as a function of the magnitude of the magnetic field passing through the MR fluid. This clutch offers the advantage of decoupling input inertia from output, resulting in a low-inertia actuator, and consequently, high bandwidths and low back-driving torque.

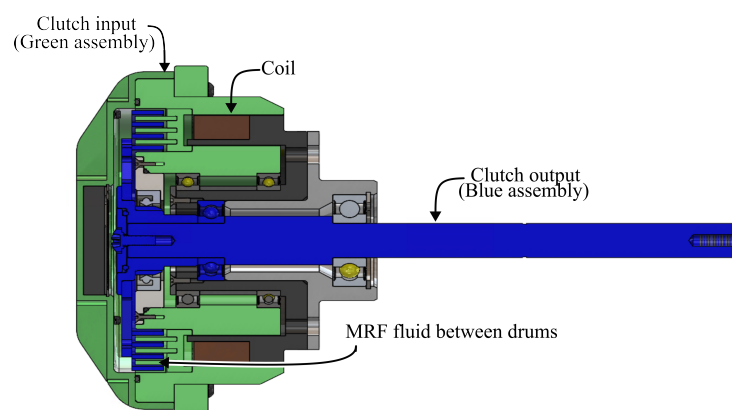


**Figure 1.** Magnetorheological (MR) clutch section view.

MR actuators were studied in an active suspension system by East et al. in a BMW 330ci car using Exonetik Inc. clutches. The design proposes counter-rotating MR clutches to provide upward and downward force with a peak force of  $\pm 5300$  N and a blocked-output bandwidth of 92 Hz. The clutches are powered by a brushless motor and the force is outputted through a gearbox, two pinions and a rack [11]. The system is packaged in a single assembly mounted on each front vehicle wheel. This study shows that MR actuators have better force density and speed compared to most current active suspensions.

Today, there is no hydrostatic active suspension system capable of generating sufficient force to manage heavy vehicle mass, while having a sufficient bandwidth to mitigate the first frequency mode harmful to the human body. This paper has the objective to explore whether an MR hydrostatic actuator system has the force and frequency performance needed to potentially manage heavy vehicle vibrations. The approach to reach this objective is to build a real-life prototype that is tested in laboratory conditions following the design requirements of a representative case study vehicle: John Deere 6R 120 farming tracked tractors as seen in Figure 2. Tracked tractors are becoming more popular due to the traction advantage they provide, as well as a better soil compaction performance resulting from their larger contact patch [12]. However, track systems are rigid systems with limited damping elements compared to tires, resulting in vibration propagation to the operator. The tractor is equipped with a conversion track system (CTS). The vibration reduction approach is to actively control vibrations on the system by modulating track tension. The production track system is equipped with a passive hydrostatic cylinder. The proposed actuator design replaces this passive cylinder with a system capable of adding and extracting energy to control the dynamics of the track. Managing track oscillations reduces the vibrations transmitted to the tractor operator and mitigates accelerated mechanical part wear due to excessive tension. The case study used in this paper is a specific case, but the actuator could be placed to act on any vehicle with sprung or unsprung mass.



**Figure 2.** John Deere 6R 120 tractor with conversion track system (CTS).

## 2. Materials and Methods

### 2.1. Design Requirements

In this study, the target blocked-output force frequency is 20 Hz. Frequencies in the range of 1 to 20 Hz can cause the body organs, tissues, spinal column and other body components to resonate [13]. A resonance behavior study of Kitazaki et al. showed that the first principal seated human body resonance frequency is about 5 Hz, and the second principal is about 8 Hz [7]. The output target force is 10 kN to control case study tractor CTS vibrations.

### 2.2. Proposed Actuator Design

The proposed actuator design is a hydrostatic system driven by electric motors and MR clutches capable of generating high force at an end effector (slave cylinder). The components are illustrated in Figure 3. Two high-speed, high-power (7.2 kW continuous, 12.9 kW peak power) brushless electric motors independently drive two Exonetik clutches. The actuator force depends on the torque transmitted by the clutches to the rack. The torque varies as

a function of the current sent to the clutch coil which varies between 0 and 14 A. At 0 A, the clutch input and output are disconnected and the rack can be back-driven with the clutch output turning freely. At maximum current, the torque transmitted is close to 37 N·m. The use of MR clutches makes the system back-drivable since the input and output can be completely disconnected when no current is sent to the clutches. The outputs of the clutches are connected by reduction gears to pinions driving a single rack. The two clutches can work in an antagonistic configuration to push and pull on the rack, or they can act in the same direction to provide maximal force in one direction. The antagonistic configuration's main advantage is to switch direction of the rack quickly with the activation and deactivation of the clutches. The synergistic configuration is used to output maximal actuator force. The rack is connected to a master hydraulic cylinder rod acting on a slave cylinder. A nitrogen-filled piston accumulator is linked to the master cylinder, acting like a spring to apply force to the slave cylinder. The actuator design characteristics are presented in Table 1.

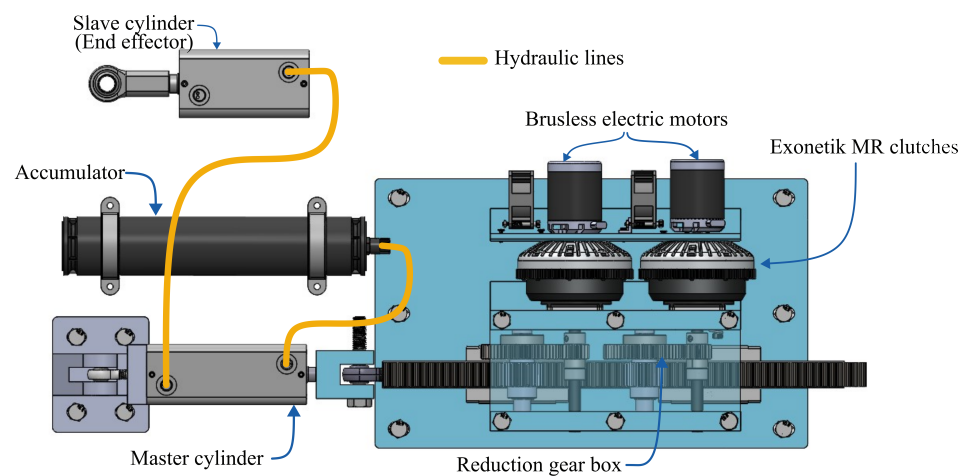


**Figure 3.** MR actuators test bench diagram.

### 2.3. Hydraulic System

The hydraulic system is composed of two hydraulic cylinders and one nitrogen piston accumulator to output high force at the end effector (slave cylinder rod). The schematic is shown in Figure 4. The slave and master cylinder bore diameter difference represents a force ratio of 1.25. The accumulator applies a quasi-constant force to the slave cylinder independently of its piston position because of its small radius-to-length ratio. The MR actuator can modulate that force by adding or removing force to the slave piston. The way the two force components acts is shown in Figure 5. The accumulator and MR actuator work in parallel to apply force to the slave cylinder. To achieve the 10 kN at the end effector for the case study vehicle, the system is designed so that about 75% of that force is coming from the accumulator stored energy, while 25% is required by the MR actuators. The slave cylinder is remotely positioned to act on a heavy vehicle frame but could actuate various dynamic systems. The remaining components of the actuator system are packaged in a single system that can be positioned strategically on the vehicle. A hydraulic hose is connected between the two system components.

**Table 1.** Test bench specifications.

Actuator Test Bench	
Dimensions	
Overall dimensions	(0.9 × 0.4 × 0.2) m
Estimated weight	~40 kg
Calculated theoretical inertia reflected in output referential	~24 kg
Actuator stroke (slave cylinder)	80 mm
Hydraulic	
Master cylinder	Parker 32MCHDBR4M115
Slave cylinder	Parker 40MCHDBR4M80
Hose	9.52 mm (3/8") SAE 100R17
Oil	AW46
Accumulator	
Accumulator	Parker ACP04AA050-0020
Gas	Nitrogen
Gas volume	0.5 L
Working pressure	27.5 MPa
Preload pressure	2.6 MPa
Electric motor	
Model	KDE700XF-295-G3
Type	Single-rotor brushless motor
Batteries	MaxAmps LiPo 9000 mA 8S2P 29.6 V battery pack
Drives	Flier R-Snake ESC 16S LiPo 400 A
Magnetorheological (MR) clutches	
Model	Exonetik Inc. (US 2018/0156285)
Max torque	37 N·m *
Peak power	24 kW *
Viscous torque	0.06 N·m·rad <sup>-1</sup> s *
Weight per clutch	4.4 kg *
Output inertia	20 kg·mm <sup>2</sup> *
Drives	Advanced motion controls 25A8
Mechanical parts	
Rack	Misumi MRGF2.5-500
Pinion	QTC KMSGB2.5-15
18 teeth gear (gear box)	QTC KMSGB1.5-18
55 teeth gear (gear box)	QTC KMSG1.5-55
Motor output gear	QTC KSS 1-16
Ring gear	QTC KSS1-120
Linear guide rail	THK SHS30-520L
Linear guide block	THK SHS30R1SS
Test hardware	
Controller	Speedgoat Performance real-time machine with Matlab Simulink
Traction machine	MTS TestFrame 322 (Flextest SE controller)
String potentiometer	McMaster string potentiometer 6863K3
Load cell	MTS 661.20.E-03

\* Values from reference [11].

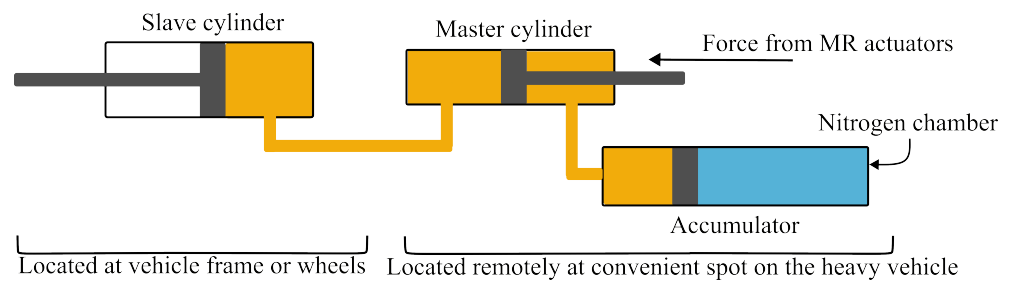


**Figure 4.** Actuator hydraulic diagram.

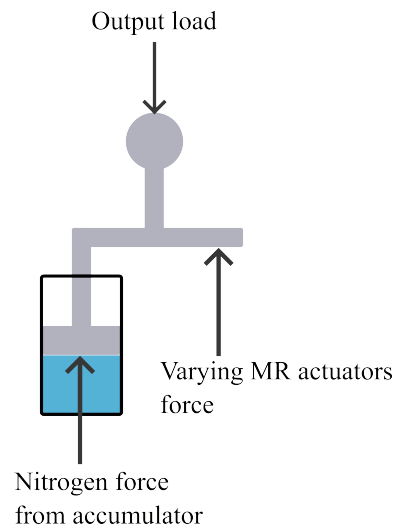


**Figure 5.** Sum of forces acting on the end effector.

#### 2.4. MR Actuators

The MR actuators are responsible for outputting high force to the rack and pinion. The two brushless electric motors are powered by a battery pack of 59 V to output individually a maximum torque of 4.7 N·m. There is a first reduction between the motor and clutch ring gear of ratio 7.5. The clutch outputs are linked to the rack through a gearbox of ratio  $\sim 3$  and a pinion resulting in a theoretical force of about 6.9 kN transmitted to the rack by each motor. The system is designed to need about 2 kN of the MR actuator to achieve 10 kN at the end effector for the case study vehicle. The clutches from Exonetik have specifications that exceed the case study vehicle needs, but it could be used on any vehicle requiring higher peak forces to control dynamics.

The main perk of using MR clutch is the low output inertia. The use of a fluid between input and output clutch drums disconnects the output from the input inertia. The clutch output rotational inertia is 20 kg·mm<sup>2</sup> [11]. This setup can output high force at a higher bandwidth than most classic hydrostatic systems.

#### 2.5. Description of the Analytical Model

##### 2.5.1. Two-Degree-of-Freedom Analytical Model

A two-degree analytical model of the actuator system was developed to ensure that the design has a first resonance mode above the 20 Hz target, at least, theoretically. Figure 6 shows the equivalent mechanical system of the MR active suspension system as a mass–spring–damper system.

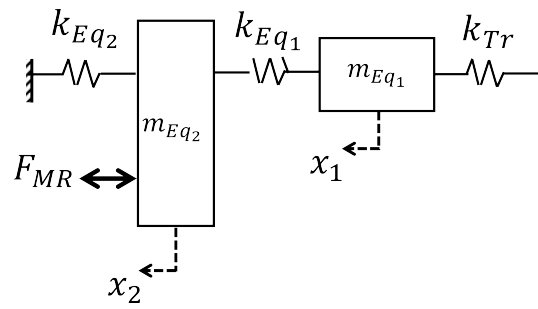


**Figure 6.** Actuator represented as a two-degree-of-freedom mass–spring–damper system.

The governing dynamic equation of motion of the system can be written as:

$$m_{Eq1} \ddot{x}_1 + (k_{Tr} + k_{Eq1})x_1 - k_{Eq1}x_2 = 0, \quad (1)$$

$$m_{Eq2} \ddot{x}_2 + (k_{Eq1} + k_{Eq2})x_2 - k_{Eq1}x_1 = F_{MR}, \quad (2)$$

where  $F_{MR}$  represents the force provided by the electric motor and transferred from the clutch input to the clutch output. The torque transferred from the clutch varies as a function of the current sent to the clutch coil. This relationship is not directly proportional due to the MRF having a complex behavior, according to Ref. [14]. Parameter  $x_1$  and  $x_2$  are the displacements of the slave and master pistons, respectively. Parameter  $m_{Eq1}$  represents the combined equivalent masses of the slave piston  $m_s$  and the hydraulic transmission fluid and  $m_{Eq2}$  is the combined equivalent mass of the MR clutch, gear box and rack, master piston  $m_m$ , hydraulic transmission fluid  $m_{Eqoil_2}$  and hydraulic transmission fluid in the accumulator  $m_{oil_{Ac}}$ . The parameter  $k_{Tr}$  is the stiffness of the rubber track. The parameter  $m_{Eq1}$  is expressed as the sum of the moving piston mass of the slave cylinder and the equivalent mass of the hydraulic transmission fluid as follows:

$$m_{Eq1} = m_m + m_{Eqoil_1}. \quad (3)$$

The parameter  $m_{Eqoil_1}$  is obtained considering the conservation of total kinetic energy [15]:

$$\frac{1}{2}m_{Eqoil_1}v_s^2 = \frac{1}{2}m_{oil_s}v_s^2 + \frac{1}{2}0.5m_{oil_h}v_{oil_h}^2, \quad (4)$$

where  $v_s$  and  $v_{oil_h}$  are the velocities of the fluid in the slave cylinder and the connecting hose, respectively. The parameters  $m_{oil_s}$  and  $m_{oil_h}$  are the fluid mass in the slave cylinder and connecting hose. Assuming that the volume flow is constant in the cylinders and in the hose, the velocities are related as:

$$v_{oil_h}A_h = v_sA_s. \quad (5)$$

Using Equations (4) and (5),  $m_{Eqoil_1}$  is obtained as:

$$m_{Eqoil_1} = \rho_{oil} \left( A_s L_s + 0.5 A_h L_h \frac{D_s^4}{D_h^4} \right), \quad (6)$$

where  $\rho_{oil}$  is the density of the hydraulic transmission fluid.  $D_s$ ,  $A_s$  and  $L_s$  are the slave cylinder effective diameter, effective area and stroke, respectively.  $D_h$ ,  $A_h$  and  $L_h$  are the hose internal diameter, internal area and length, respectively.

Similarly,  $m_{Eq2}$  can be evaluated as follows:

$$m_{Eq2} = I_{output} + m_m + m_{Eqoil_2} + m_{oil_{Ac}}, \quad (7)$$

$$m_{E_{oil_2}} = \rho_{oil} (A_m L_m + 0.5 A_h L_h \frac{D_m^4}{D_h^4}), \quad (8)$$

where subscript  $m$  represents the master cylinder and  $I_{output}$  represents the inertia of clutch output, gear box, rack and rail, referenced in the master cylinder axle.  $m_{oilAc}$  is the sum of the oil mass in the accumulator side of the master cylinder and the accumulator oil.

Parameter  $k_{Eq_1}$  represents the hydraulic stiffness of the master and slave cylinder including the rigidity of the fluid  $k_{bulk_1}$  and radial rigidity of the hydraulic hose  $k_{hose}$  as follows [15]:

$$\frac{1}{k_{Eq_1}} = \frac{1}{k_{bulk_1}} + \frac{1}{k_{hose}}, \quad (9)$$

where

$$k_{bulk_1} = \frac{A_s^2 B_{oil}}{A_s L_s + A_h L_h + A_m L_m}, \quad (10)$$

$$k_{hose} = \frac{\pi P_s D_m^4}{4 L_h \left( \frac{P_s D_{hm}^3}{t_h E_h} + \left( \frac{P_s D_{hm}^2}{2 t_h E_h} \right)^2 \right)}. \quad (11)$$

$B_{oil}$  is the bulk modulus of the hydraulic oil and  $P_s$  is the absolute oil pressure in the slave cylinder.  $D_{hm}$ ,  $t_h$  and  $E_h$  are hose mean diameter, wall thickness, and Young's modulus, respectively.

Similarly, the equivalent hydraulic stiffness of the accumulator and master cylinder  $k_{eq_2}$  is obtained as follows:

$$\frac{1}{k_{Eq_2}} = \frac{1}{k_{bulk_2}} + \frac{1}{k_{gas}}, \quad (12)$$

where

$$k_{bulk_2} = \frac{A_{mG}^2 B_{oil}}{A_{mG} L_{mG} + V_{Ac_{oil}}}, \quad (13)$$

$$k_{gas} = \frac{P_{mG}^2 A_{PG}^2}{V_{AC_{gas}} (P_{mG} - P_{atm})}. \quad (14)$$

$A_{mG}$  and  $L_{mG}$  are the effective area and length of the master cylinder on the accumulator side, respectively, and  $V_{Ac_{oil}}$  is the oil volume in the accumulator. Parameter  $k_{gas}$  represents the stiffness of the gas side of the accumulator, which is calculated as a function of the oil pressure of the master cylinder on the gas side  $P_{mG}$ , volume of the gas in the accumulator  $V_{AC_{gas}}$  and effective area of accumulator piston  $A_{PG}$ . The equation assumes there is no air trapped in the oil, the hose material has an isotropic behavior and there is no hydraulic viscous force causing head loss.

To evaluate the system's natural frequency, the parameters in Table 2 are used. The Equations (1) and (2) can be written in a state space as the following equation:

$$[\dot{x}] = [A][x], \quad (15)$$

with  $A$  as the following matrix

$$[A] = \begin{bmatrix} 0 & 1 & 0 & 0 \\ \frac{-(k_{Eq_1} + K_{Tr} + k_{Return})}{m_{Eq_1}} & 0 & \frac{k_{Eq_1}}{m_{Eq_1}} & 0 \\ 0 & 0 & 0 & 1 \\ \frac{k_{Eq_1}}{m_{Eq_2}} & 0 & \frac{-(k_{Eq_1} + k_{Eq_2})}{m_{Eq_2}} & 0 \end{bmatrix}. \quad (16)$$



The eigenvalues ( $\lambda$ ) are found with the solution of the following equation:

$$|A - \lambda I| = 0, \quad (17)$$

where  $I$  is an identity matrix of matrix  $A$  size. The equation solution gives eigenvalues ( $\lambda$ ) with the imaginary part being the system's natural frequency.

### 2.5.2. One-Degree-of-Freedom Analytical Model

For the purpose of this article, the model used to represent the blocked-output conditions in the laboratory is a simplified version of the model described above. The experimental setup explained in Section 3.1 cannot be correctly represented by the two-degree model described above because of the blocked-output configuration. This one-degree model is used to compare the parameters with the experimental data and evaluate the system's natural frequency. The model is presented in Figure 7.

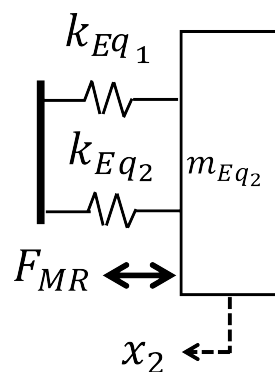


Figure 7. One-degree-of-freedom model of the actuator system.

In this blocked-output configuration, the dynamic equation of motion simplifies to:

$$m_{Eq2} \ddot{x}_m - x(k_{Eq1} + k_{Eq2}) = F_{MR}. \quad (18)$$

With the same procedure described in Section 2.5.1, it is possible to estimate the system's natural frequency with the resulting equation:

$$f = \sqrt{\frac{k_{Eq1} + k_{Eq2}}{m_{Eq2}}}. \quad (19)$$

### 2.5.3. Analytical Model Results

The one-degree analytical model predicts a first mode at 78 Hz. It is important to note that some parameters are estimated because of their complexity, like the hose Young's modulus that is actually composed of two materials: rubber and steel braiding. The model also assumes that the mounting of the actuator system is completely rigid, and the piston and rod mass were estimated from known data.

**Table 2.** Parameters used in analytical model.

Hose		
$\phi_H$	Hose internal diameter	9.52 mm
$D_H$	Hose mean diameter	13.02 mm
$t_H$	Hose thickness	3.50 mm
$E_H$	Hose Young's modulus	4–10 GPa *
$A_H$	Hose internal area	71.18 mm <sup>2</sup>
$L_H$	Hose length	1.83 m
Cylinders		
$D_s$	Slave piston diameter	40 mm
$A_s$	Slave piston area	1257 mm <sup>2</sup>
$L_s$	Slave cylinder stroke	80 mm
$M_s$	Slave piston mass	0.67 kg
$D_m$	Master piston diameter	32 mm
$A_m$	Master piston area	804.3 mm <sup>2</sup>
$L_m$	Master cylinder stroke	115 mm
$M_m$	Master piston mass	0.26 kg
Oil		
$\rho_o$	Mineral oil density	875 kg·m <sup>-3</sup>
$B_o$	Oil bulk modulus	2.07 GPa
$V_s$	Oil volume in slave cylinder	$1.01 \times 10^{-4}$ m <sup>3</sup>
$V_m$	Oil volume in master cylinder	$9.25 \times 10^{-5}$ m <sup>3</sup>
$V_{Ac}$	Oil volume in accumulator	$5.08 \times 10^{-4}$ m <sup>3</sup>
$V_H$	Oil volume in hose	$1.3 \times 10^{-4}$ m <sup>3</sup>
Inertia of mechanical components in rack gear reference		
$I_{Clutch}$	Clutch inertia	0.53 kg
$I_{gear}$	Gear box inertia	4.11 kg
$I_{rack}$	Rack and rail inertia	5.05 kg

\* Values from reference [16].

### 3. Results and Discussion

#### 3.1. Experimental Test Bench

The hydrostatic MR actuator was tested to validate the system performance. The slave cylinder was mounted on a MTS traction machine as shown in Figure 8, and the rest of the actuator system was relocated to the side of the machine. For the majority of the tests, the slave cylinder was put in a blocked-output configuration on the MTS machine. The electric motor was driven at 4000 RPM because it maximizes its torque value and thus corresponds to a 530 RPM clutch slip speed. In addition to this parameter, a positive slip between the input and output is wanted to assure a quick response from the actuator. The value of this slip induces a higher power consumption because the slip energy is dissipated as heat, which amounts to 2.05 kW for the clutch maximum torque of 37 N·m. This is not a challenge for the purpose of these tests but should be taken into consideration for extended use. The two clutches are denoted by Clutch A and Clutch B for the rest of the discussion.

All tests were controlled by a Speedgoat Performance acquisition system paired with Matlab Simulink software, allowing high frequency control. The electric motors were driven by Flier drives and the clutches were driven by Advanced Motion Controls drives.

Two hall effect sensors read motor speed, allowing a proportional-integral-derivative (PID) controller to regulate the motor speed with a closed-loop control. Two string potentiometers were located on the master and slave cylinders and provided displacement. The MTS machine's load cell was used to monitor force on the slave cylinder.

The accumulator was preloaded with a pressure of 2.6 MPa. When the slave cylinder was mounted on the MTS traction machine, a manual hydraulic pump was used to pressurize the hydraulic hose of the accumulator at 8 MPa, resulting in a preload force of 6800 N

at the slave cylinder. Note that in the case of the study vehicle, this operation would be performed with the use of the tractor's power from take-off as this is already the method used for tensioning the track.

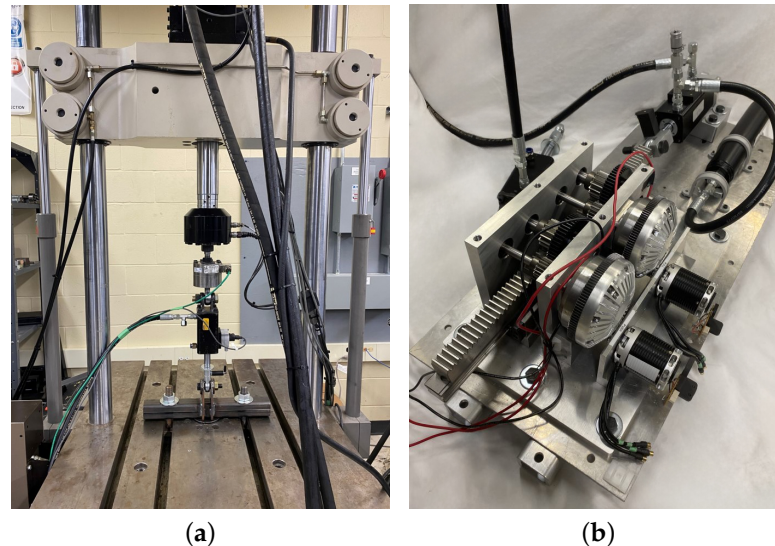


**Figure 8.** Physical test bench on MTS machine. (a) Slave cylinder on MTS traction machine. (b) Actuator test bench.

### 3.2. Clutch Characterization and Hysteresis

The first test performed on the MTS machine was the characterization of the output force at the slave piston as a function of the current induced in the coil of each clutch. To perform the test, the electric motor was running at a constant speed and a current triangle function (ramp-up and ramp-down) of 6 s was sent to the clutch coil. While the clutches coils are rated to a maximum of 14 A peak, the current sent to the clutches was limited to 9 A for clutch A and 10 A for clutch B. That limit was set for safety reasons and 10 A was not reached for clutch A because it required too high a battery power demand. The tests were performed separately for each clutch in a push configuration.

The result is a force curve as a function of current as presented in Figure 9. The preload force of 6.8 kN on the slave cylinder is subtracted from the load cell force data to exclude its influence. Clutch A has a maximal force of 8.28 kN at 9 A, while clutch B has a maximal force of 8.47 kN at 10 A. The difference in performance is expected since the fabrication process of the clutches implies some variability. For instance, the two clutches have coils of different sizes, so there are different clearances between clutch drums and friction may differ between the parts.

Hysteresis is noticeable on the graphs and is around 25% of the maximum force. The authors suspect that most of the hysteresis is due to the piston seals because it is in the range of the Coulomb friction measured on the system, as seen in Section 3.4. However, some of this hysteresis could be caused by magnetic hysteresis of the clutch as it is typical for MR clutches. It must be noted that the hysteresis may be higher in an application where the end effector is not in a blocked-output configuration.

With a preload on the accumulator hose of 8 MPa, clutch A and B can, respectively, induce a force of 15.68 kN and 15.63 kN on the slave cylinder.

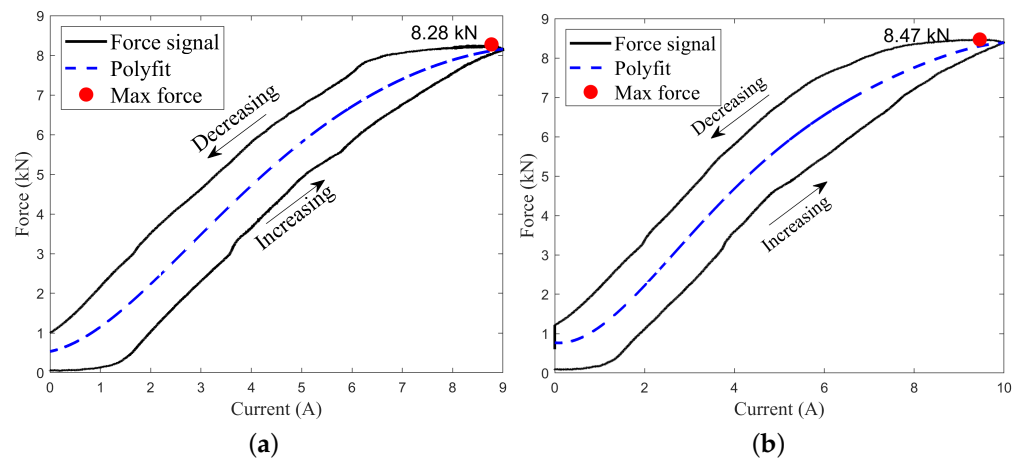


**Figure 9.** Result of clutch force characterization. (a) Force as a function of current for clutch A. (b) Force as a function of current for clutch B.

### 3.3. Blocked-Output Bandwidth

The blocked-output bandwidth test was performed by sending a chirp signal ( $\pm 3000$  N, 0.1–200 Hz, 100 s) of force to the clutches. The clutches were put in an antagonistic configuration, meaning clutch A was pushing on the rack while clutch B was pulling on the rack. The two electric motors were running at a constant speed and clutch A was activated during the positive part of the sinus chirp, while clutch B was activated during the negative part. The frequency response of output force over current input is shown in Figure 10. The Bode plot shows a 20 Hz bandwidth (based on a  $-135^\circ$  phase limit). The graph displays the raw data of the input command and force measured by the load cell. The blocked-output bandwidth matches the required 20 Hz target specification needed to control vibrations harmful to the human body. During testing, it was also observed that the system test bench lacks mechanical rigidity. The brackets and main plate were flexing. Increasing rigidity would possibly result in a higher force ratio transferred to the end effector.

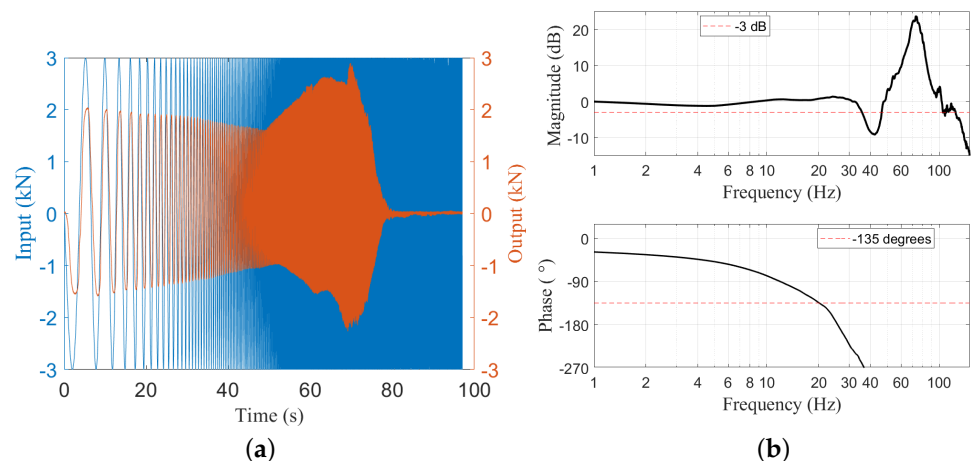


**Figure 10.** Blocked-output bandwidth test results. (a) Raw data of input command and output force. (b) Bode diagram of the system frequency response.

The Bode plot shows a clear resonance mode at 73 Hz. Compared to the analytical model of Section 2.5.3, the first natural frequency of the experimental system is rather close to the predicted value of 78 Hz. This suggests that the test bench bandwidth is limited by its flexibility but may be higher if the mounting was stiffer. However, this result should be treated with caution. Some parameters in the analytical calculation have a high margin of error, such as the hose Young's modulus and oil bulk modulus. To have a better idea of

the concordance between the analytical and experimental data, more experiments should be performed.

Furthermore, the master cylinder potentiometer data were analyzed during a clutch characterization test. For a 6.8 kN force on the master cylinder, the rod had a displacement of 2.1 mm. With this data point, it is possible to approximate a more accurate rigidity  $k_{eq2}$  in the analytical model from Section 2.5.3. With this rigidity, the model still predicts a first mode around 70–80 Hz, which supposes that the hydraulic mode caused the resonance in the experimental data. Knowing with relative confidence that the system theoretical frequency is around 70–80 Hz, it is suspected that the bandwidth is limited by the test bench rigidity. It seems that the lack of rigidity induced an over-damped second-order resonant peak in the range of 10 to 30 Hz that can be assumed since the phase shifts to 180°. With rigidity improvement and control tuning, the actuator has the potential to approach the analytical first mode predicted.

### 3.4. Friction

A friction test was performed with the use of the MTS machine. The MTS hydraulic cylinder was back-driving the actuator in displacement with sinus signals of amplitude  $\pm 20$  mm and frequencies of 0.2 Hz, 0.5 Hz, 1 Hz and 1.5 Hz while the components were free to move. No current was sent to the clutches and the motors were not running. Displacement and force were monitored by the MTS traction machine acquisition system. The results are shown in Figure 11.

The static model is found with a linear regression of the force to displacement data for each frequency seen in Figure 11a. The static friction  $f(q)$  (kN) is modeled as a one-degree function as follows with  $q$  (mm) being the cylinder displacement:

$$f(q) = 0.06q + 0.15. \quad (20)$$

The static friction reached about 1.35 kN for a displacement of 20 mm. The curve is shown in Figure 11b for the 1.5 Hz test as well as the result of force as a function of displacement. This friction value can be explained by the hydraulic system that generates much friction caused by the seal and hydraulic line rigidity.

The difference between this static friction linear equation and the force to displacement data gives the friction force as a function of speed and is shown in Figure 11c. A continuous non-linear friction model introduced by Makkar [17] is fitted on data with the parameterizable equation as follows:

$$f(\dot{q}) = \gamma_1(\tanh(\gamma_2\dot{q}) - \tanh(\gamma_3\dot{q})) + \gamma_4\tanh(\gamma_5\dot{q}) + \gamma_6\dot{q}. \quad (21)$$

A fit with the 1.5 Hz model gives the following equation:

$$f(\dot{q}) = 1.92 (\tanh(1.03 \dot{q}) - \tanh(9.5 \cdot 10^{-1} \dot{q})) + 3.58 \cdot 10^{-19} \tanh(2.36 \dot{q}) + 1.93 \cdot 10^{-2} \dot{q}. \quad (22)$$

The model is shown in Figure 11d. Modeling friction with this equation is interesting because it allows us to model the system's friction behavior, including Stribeck friction, Coulomb friction and damping in only one continuous equation. This model could be used in future work for control with friction compensation.

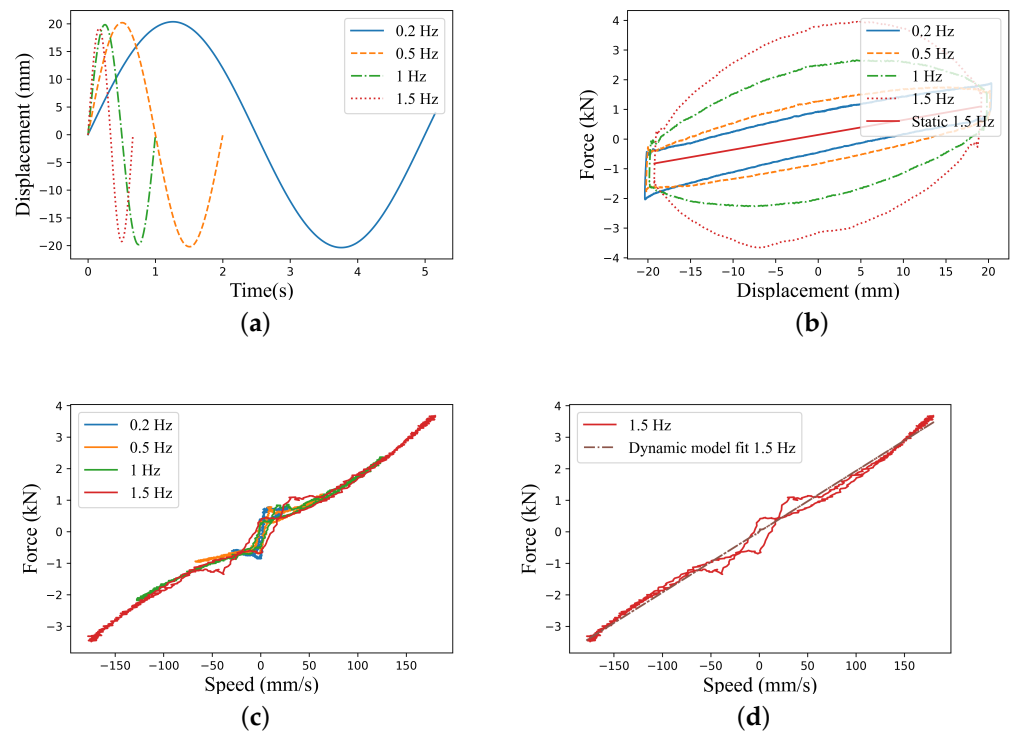


**Figure 11.** Friction test data and results. (a) MTS machine sine displacement input. (b) MTS machine cylinder force as a function of MTS cylinder displacement. (c) Friction force as a function of MTS cylinder speed. (d) Force as a function of MTS cylinder speed (1.5 Hz test) and model fit.

#### 4. Conclusions

This paper presents the design and experiment validation of a high force, high-bandwidth MR actuator having the potential to control heavy vehicle vibrations. The design includes two MR clutches that can be driven in a synergistic or antagonistic configuration, combined with a hydrostatic system that can multiply end effector force as needed for given applications.

The actuator system was tested on an MTS traction machine in a blocked-output configuration to test peak force and frequency bandwidth. The system outputs 15.6 kN of force per clutch with a preloaded accumulator of 8 MPa and a current of 10 A applied to the clutch. The clutch coils can take up to 14 A, thus potentially allowing higher output force. The synergistic use of the clutches could induce a peak force over 30 kN at the end effector. The blocked-output bandwidth test results in a phase-limited value of 20 Hz ( $-3$  dB and  $-135^\circ$  phase margin). This bandwidth matches the target value (20 Hz) that is deemed necessary to control vibrations that are harmful to the human body. The preliminary experiment shows that the system could have the potential to be an effective solution to control heavy vehicle dynamics.

The MR system compares favorably with other technologies, with a bandwidth that is higher than most hydraulic systems ( $<5$  Hz). The peak force of 15.6 kN, with the potential of a higher value with a different accumulator preload and clutch peak current could be enough to act on the sprung mass of some heavy vehicles.

The scope of this paper was to assess the performance on a test bench of MR actuators combined with hydraulics for future vibration control. Future work will include vibration simulations with the dynamic model verified by the experimental data and a feedback control strategy to test vibration control. Next steps will be the mounting of the actuator on a vehicle and testing in real terrain conditions. Finally, future work will include testing multiple control strategies in pairs with sensors and closed-loop control to achieve semi-active or active control of vibration.

**Author Contributions:** Conceptualization and design, G.M., M.H. and J.-S.P.; Methodology: G.M.; Validation: G.M. and C.-É.G.; Formal analysis: M.H., J.D. and G.M.; Investigation: G.M., C.-É.G. and J.D.; Resources: J.-S.P.; Software: G.M. and M.H.; Supervision: J.-S.P.; Visualization: G.M.; Writing—original draft: G.M. and M.H.; Writing—review and editing: G.M., J.D., C.-É.G. and J.-S.P. All authors have read and agreed to the published version of the manuscript.

**Funding:** This research was funded by Michelin, Natural Science and Engineering Research Council of Canada (CRSNG), Fonds de recherche du Québec—Nature et technologies (FRQNT) and MITACS.

**Data Availability Statement:** The data presented in this study are available on request from the author.

**Acknowledgments:** The authors would like to thank William East and Jérôme Turcotte for their past studies that led to this project and for their technical assistance. The authors would also like to thank Michelin for the opportunity and support during the research.

**Conflicts of Interest:** The authors declare no conflict of interest.

## Abbreviations

The following abbreviations are used in this manuscript:

CTS	Conversion track system
DC	Direct current
DOAJ	Directory of open access journals
EAVC	Electromagnetic active vibration cancelling
MDPI	Multidisciplinary Digital Publishing Institute
MR	Magnetorheological
MRF	Magnetorheological fluid
PID	Proportional-integral-derivative
WBV	Whole-body vibration

## References

- Upadhyay, R.; Bhattacharjee, A.; Patra, A.K.; Chau, N. Association between Whole-Body Vibration exposure and musculoskeletal disorders among dumper operators: A case-control study in Indian iron ore mines. *Work* **2022**, *71*, 235–247. [CrossRef] [PubMed]
- Singh, A.; Samuel, S.; Singh, H.; Singh, J.; Prakash, C.; Dhabi, Y.K. Whole Body Vibration Exposure among the Tractor Operator during Soil Tillage Operation: An Evaluation using ISO 2631-5 Standard. *Shock Vib.* **2022**, *2022*, 6412120. [CrossRef]
- Kaewunruen, S.; Remennikov, A.M. Current state of practice in railway track vibration isolation: An Australian overview. *Aust. J. Civ. Eng.* **2016**, *14*, 63–71. [CrossRef]
- Chouinard, P.; Begin, M.A.; Fortin, J.M.; Berry, A.; Masson, P.; Plante, J.S. Preventing lower back pain among truck drivers: Design and performance of a controlled slippage magnetorheological actuator for an active seat suspension. In Proceedings of the ASME 2018 International Design Engineering Technical Conferences and Computers and Information in Engineering Conference, IDETC/CIE, Quebec City, QC, Canada, 26–29 August 2018; Volume 5A-2018. [CrossRef]
- Davies, H.W.; Wang, F.; Du, B.B.; Viventi, R.; Johnson, P.W. Exposure to Whole-Body Vibration in Commercial Heavy-Truck Driving in On- and Off-Road Conditions: Effect of Seat Choice. *Ann. Work Expo. Health* **2022**, *66*, 69–78. [CrossRef] [PubMed]
- Lee, J.; Oh, K.; Yi, K. A novel approach to design and control of an active suspension using linear pump control-based hydraulic system. *Proc. Inst. Mech. Eng. Part D J. Automob. Eng.* **2020**, *234*, 1224–1248. [CrossRef]
- Kitazaki, S.; Griffin, M.J. Resonance behaviour of the seated human body and effects of posture. *J. Biomech.* **1997**, *31*, 143–149. [CrossRef] [PubMed]
- Mercedes-Benz Pioneers Fully Active Suspension. Available online: <http://media.mercedes-benz.ca/releases/mercedes-benz-pioneers-fully-active-suspension> (accessed on 21 September 2023).
- Fauteux, P.; Lauria, M.; Legault, M.A.; Heintz, B.; Michaud, F. Dual differential rheological actuator for robotic interaction tasks. In Proceedings of the 2009 IEEE/ASME International Conference on Advanced Intelligent Mechatronics, Singapore, 14–17 July 2009; pp. 47–52. [CrossRef]
- Veronneau, C.; Denis, J.; Lebel, L.P.; Denninger, M.; Plante, J.S.; Girard, A. A Lightweight Force-Controllable Wearable Arm Based on Magnetorheological-Hydrostatic Actuators. *arXiv* **2019**, arXiv:2206.13361.
- East, W.; Turcotte, J.; Plante, J.S.; Julio, G. Experimental assessment of a linear actuator driven by magnetorheological clutches for automotive active suspensions. *J. Intell. Mater. Syst. Struct.* **2021**, *32*, 955–970. [CrossRef] [PubMed]
- Arvidsson, J.; Westlin, H.; Keller, T.; Gilbertsson, M. Rubber track systems for conventional tractors – Effects on soil compaction and traction. *Soil Tillage Res.* **2011**, *117*, 103–109. [CrossRef]

13. Eger, T.; Stevenson, J.; Boileau, P.E.; Salmoni, A. Predictions of health risks associated with the operation of load-haul-dump mining vehicles: Part 1-analysis of whole-body vibration exposure using iso 2631-1 and ISO-2631-5 standards. *Int. J. Ind. Ergon.* **2008**, *38*, 726–738. [[CrossRef](#)]
14. Lucking Bigué, J.P.; Charron, F.; Plante, J.S. Understanding the super-strong behavior of magnetorheological fluid in simultaneous squeeze-shear with the Péclet number. *J. Intell. Mater. Syst. Struct.* **2015**, *26*, 1844–1855. [[CrossRef](#)]
15. Veronneau, C.; Bigue, J.P.L.; Lussier-Desbiens, A.; Plante, J.S. A High-Bandwidth Back-Drivable Hydrostatic Power Distribution System for Exoskeletons Based on Magnetorheological Clutches. *IEEE Robot. Autom. Lett.* **2018**, *3*, 2592–2599. [[CrossRef](#)]
16. Hruik, L.; Bureek, A.; Vaina, M. Mathematical simulation and measurement of expansion of hydraulic hose with oil. *Teh. Vjesn. Gaz.* *24*, 1905–1914. [[CrossRef](#)]
17. Makkar, C.; Dixon, W.; Sawyer, W.; Hu, G. A new continuously differentiable friction model for control systems design. In Proceedings of the 2005 IEEE/ASME International Conference on Advanced Intelligent Mechatronics (IEEE Cat. No. 05TH8801), Monterey, CA, USA, 24–28 July 2005; Volume 1, pp. 600–605.

**Disclaimer/Publisher’s Note:** The statements, opinions and data contained in all publications are solely those of the individual author(s) and contributor(s) and not of MDPI and/or the editor(s). MDPI and/or the editor(s) disclaim responsibility for any injury to people or property resulting from any ideas, methods, instructions or products referred to in the content.